EVOLUTION
INTERNATIONAL JOURNAL OF ORGANIC EVOLUTION
SSE
SOCIETY for the STUDY of EVOLUTION

Linking modularity and conspicuous asymmetry in the insect head and mandibles.

Journal:	*Evolution*
Manuscript ID	EVO-23-0489
Manuscript Type:	Original Article
Keywords:	Bite force, Covariance ratio, EMMLi, geometric morphometrics, 3D landmarks, Orthoptera

Linking modularity and conspicuous asymmetry in the insect head and mandibles.

Abstract. Bilateral symmetry is widespread across animals, yet, among bilaterians, many cases of conspicuous asymmetries evolved. This means that bilaterally homologous structures on the left and right side display divergent phenotypes. Evolution of such divergent phenotypes between otherwise similarly shaped structures can be thought to be favoured by modularity, but this has rarely been studied in the context of left-right differences. Here, we provide an empirical example, using geometric morphometrics, to assess patterns of asymmetry and variational modularity, i.e., covariation patterns between landmark partitions, in a grasshopper with conspicuously asymmetric mandibles. Our morphometric data confirms the presence of conspicuous directional asymmetry in the mandibles, and surrounding structures, but not in the dorsal half of the head, which carries sensory structures. The strongest modularity signal is found between a single module, composed of both mandibles, and the rest of the head, which is best explained by a combination of functional (feeding vs. sensory) and developmental (different ontogenetic origins) modularity. Left and right mandibles also show significant, albeit weaker, variational modularity. This supports the idea that developmental modularity may allow asymmetric shapes of left and right mandibles to arise, while these remain integrated, resulting in the key-and-lock morphology required for their feeding function.

Keywords. Bite force, Covariance ratio, EMMLi, geometric morphometrics, 3D landmarks, Orthoptera.

Introduction

Bilateral symmetry is one of the most widespread morphological characters in animals. Yet, even animals with a well-defined bilaterally symmetrical body plan (e.g. most bilaterians) are *not strictly* symmetrical, since many structures such as internal organs are asymmetrical or even unilateral (Babcock, 2005; Palmer, 1996; Van Valen, 1962). The break-up of symmetry can take many other forms, sometimes less evident, and with different biological implications (Klingenberg, 2022; Palmer, 1994; Van Valen, 1962). Shape differences between left and right sides can be *subtle*, requiring quantitative measurements to detect them. Among such subtle asymmetry types, fluctuating asymmetry (FA) arguably is the best studied, mostly as an assumed proxy for developmental instability, relating to intrinsic or extrinsic stresses on organisms (Benítez et al., 2020; Graham et al., 1994; Klingenberg, 2022; Møller, 1990; Palmer, 1994; Savriama et al., 2016; Van Valen, 1962). When studying fluctuating asymmetry, it is assumed that symmetry is the norm and the target phenotype to achieve (Hansen et al., 2006), and that "stressors", such as random mutations or environmental conditions, lead to small left-right differences, the distribution of which should be normal and centered on zero (i.e. on perfect symmetry) at the population level (Palmer, 1994). Subtle asymmetry types also include directional asymmetry (DA) and antisymmetry, in which a symmetrical phenotype is *not* the norm, with the left-right differences being of consistent direction in the case of directional asymmetry, leading to a normal distribution *not* centered on zero, or of random direction in antisymmetry, leading to a platykurtic or bimodal distribution of differences. Directional asymmetry and antisymmetry are also found, and are characteristic, for *conspicuous asymmetries*, which are cases of asymmetry readily visible upon observation (Babcock, 2005; Palmer, 2004).

Because directional asymmetry and antisymmetry entail systematic differences between sides, they are generally considered to be inherited, and sometimes to be adaptive (Palmer, 2004). The latter

point, however, is dependent on whether subtle or conspicuous asymmetries are studied. For example, *subtle* directional asymmetries in insect wings have been repeatedly demonstrated, but may be of little adaptive significance, due to limited functional consequences (Klingenberg et al., 1998; Pélabon & Hansen, 2008; Pither & Taylor, 2000). On the other hand, *conspicuous* directional asymmetry in the skull of toothed whales has been argued to be related to feeding or biosonar function (Churchill et al., 2019; del Castillo et al., 2016; Huggenberger et al., 2017; Laeta et al., 2023; Lanzetti et al., 2022; Macleod et al., 2007); extreme conspicuous directional asymmetry in the skulls of flatfishes relates to their benthic ecology (Evans et al., 2021); conspicuous antisymmetry in many Crustacean appendages has been related to divergent left and right functions (Govind, 1989; Govind & Blundon, 1985; Levinton, 2016; Pratt & Mclain, 2002); and in humans and mice, the mirroring of internal organs, or *situs inversus*, is mostly problematic when only some of the organs are concerned, while complete *situs inversus* entails no major health defects (Palmer, 2004).

If one considers that there is not just one left-right (or right-left) body axis, but instead two opposite medio-lateral axes (Meinhardt, 2001; Palmer, 2004), the emergence of conspicuously different left and right phenotypes can be interpreted as the relatively independent expression of two different developmental programs, which can be initiated genetically (e.g. usual *situs solitus*), randomly (e.g. *situs inversus* in *iv* mutant mice), or environmentally (e.g. lobster claws)(Brown & Wolpert, 1990; Govind, 1989; Palmer, 2016). It should however be kept in mind that even in extreme cases of antisymmetry (e.g. in fiddler crabs), the development of both sides has been shown to be positively correlated, at least in terms of resource investment (Levinton, 2016). With this view in mind, in cases of conspicuous directional asymmetry or antisymmetry both medio-lateral axes may be akin to *quasi-autonomous components* (Wagner et al., 2007; Zelditch & Goswami, 2021), producing a special case of modularity in which left and right sides of a bilaterally homologous structure represent developmental modules. In addition to being developmentally modular, each side may also sometimes represent a quasi-autonomous functional module, illustrated perhaps most obviously in male fiddler crabs which use their minor claw to feed and their major claw for fights and displays, certainly leading to very different selective pressures on the opposite sides of the animal (Pratt & Mclain, 2002). Such functional and/or developmental left-right modularity may be key in allowing bilaterally homologous structures to evolve different morphologies, and in some cases different functions (Clune et al., 2013; Wagner et al., 2007). Although the modularity of crab claws has, to our knowledge, not directly been assessed, studies on the skull of toothed whales do suggest a link between the presence of directional asymmetry and a modification of the modularity pattern of the skull (Churchill et al., 2019; del Castillo et al., 2016, 2017). The situation in this latter case is slightly more entangled than in the crab claws example, because both sides of the skull, which may develop differently, may at the same time be involved in the same function, here feeding or sound production. On the other hand, the general shape of the skull should achieve some degree of symmetry to retain hydrodynamic properties, which would require that some skull modules develop symmetrically, while others develop asymmetrically.

Another case of conspicuous asymmetry are the mandibles of many insects, and among them Orthopterans, i.e. grasshoppers, crickets and relatives (Ball, 1992; Chapman, 1964; Clissold, 2007). Mandibles are used to induce shear and crush food, and their asymmetric shapes allow the distal parts (incisivi) to cross and act as double blades, and the proximal parts (molars) to occlude, forming a key-and-lock morphology (Fig. 1) (Clissold, 2007). The left and right mandibles each rotate around an axis formed by two articulation points with the head capsule. They can move independently from each other, meaning they are by definition anatomical modules, and, in Orthopterans, they are each actuated by one adductor and one abductor muscle which are attached to the inside of the head capsule cuticle (Clissold, 2007). Contrary to the bones of the Cetacean skull, the Orthopteran

mandibles remain to a large extent physically independent from each other, while, contrary to the fiddler crab claws, both mandibles must work together to achieve efficient feeding. The Orthopteran head (including mandibles) therefore constitutes an intermediate study case of an integrated structure, or *tagma* (Minelli et al., 2013), combining symmetric and asymmetric structures: Left and right mandibles are physically independent, but work together in a key-and-lock principle, while the rest of the head capsule should be under selective pressure for symmetry, given it holds sensory structures such as the eyes and antennae. In addition to a common function, left and right mandibles share a common developmental origin (Posnien & Bucher, 2010).

We propose that (i) to achieve conspicuous asymmetry, the opposite medio-lateral axes of development must have some degree of autonomy from each other, thereby forming modules. At the same time, because head symmetry should be generally maintained, we may expect that (ii) asymmetric structures should be to some degree autonomous from symmetric ones leading to significant modularity between them, to allow for asymmetry to arise. (iii) In the case where the left and right asymmetric components must work together to achieve a common function, functional constraints may also counteract potential right-left developmental modularity suggested in point (i). Another possibility is that (iv) asymmetries may "spill-over" to neighboring areas, for example here through asymmetric mechanical loads on the head capsule (Levinton, 2016; Pratt & Mclain, 2002; Tiwari et al., 2017), which would increase correlations (and reduce modularity) between the conspicuously asymmetric structures and their anatomically linked structures.

To test these hypotheses, we focus here on the Orthopteran head and mandibles shape, which we quantify using geometric morphometrics. We measure morphological variation in adults at the population level, and decompose it into various types of asymmetries. Taking advantage of the multivariate nature of geometric morphometric data, we study covariation patterns between traits to test different *variational* modular partitions and compare them to each other (Klingenberg et al., 2001; Wagner et al., 2007; Zelditch & Goswami, 2021). We expect that mandibles should show strong directional asymmetry, as already shown qualitatively. We also expect that their asymmetrical mechanical actions may induce asymmetry in the neighboring regions, but less so in more distant regions of the head, especially around sensory structures for which symmetry is functionally advantageous (e.g. compound eyes). Second, we expect that, according to point (i), the left and right mandibles may constitute variational modules, with lower-than-expected integration between them, allowing their divergent morphologies to emerge, and that they are also quasi-autonomous with regard to the head capsule structures, in which symmetry should be maintained (point (ii)). Alternatively, because the mandibles should enable proper shearing and occlusion, it may be expected as suggested by point (iii), that they are tightly integrated, forming one functional and variational module. If this is the case, it may also be expected that the level of asymmetry is tightly controlled, showing strong adaptive accuracy (Hansen et al., 2006; Pélabon & Hansen, 2008), with individuals deviating from the optimal level of asymmetry having worse biting performance.

Materials and Methods

Specimens and measurements. Forty-nine live adult specimens of *Schistocerca gregaria* (Forskål, 1775) were purchased from Fressnapf© (Krefeld, Germany). The animals were brought back to the lab, were fed, and their maximal bite forces were measured using the setup developed by (Rühr & Blanke, 2022) on the same day or the next. Bite forces were measured by two different users (SG and SS), by holding the animals between thumb and index, and allowing them to bite voluntarily on the bite plates. Continuous sequences of bites were recorded, and the highest measured bite force

(i.e. maximal voluntary bite force) was extracted and used in further analyses. Maximum voluntary bite forces have been shown in other insects to match physiologically maximum bite forces (Püffel et al., 2023).

Fixation and microCT scanning. Specimens were then fixed in Bouin solution for ~72 hours, their heads were cut off the body, and rinsed repeatedly in 70% ethanol. Following this, the heads were dehydrated in a series of increasingly concentrated ethanol solutions, going from 70% to 100% by steps of 10%, with 1 hour at each step. After this process, the heads were critical-point dried (Tousimis Autosamdri 931.GL) before microCT using a Bruker SkyScan 1272 (voltage = 50 kV, current = 200 µA, Image pixel size = 6.0 µm or 7.5 µm) and reconstructed using NRecon. All heads had fully closed mandibles when scanned, to ensure anatomical comparability between specimens.

Landmarking. 3D reconstructed heads were imported and rendered in the software MorphoDig (Lebrun, 2018). In total, 38 homologous landmarks were placed across the head. However, three landmarks had to be excluded because they could not be placed accurately in all individuals, leaving a total of 35 landmarks (Fig. 1). All landmarks were digitized by the same user (SG) and replicated once, to allow discrimination between the various components of inter- and intra-individual shape variation (i.e. asymmetry, see below).

Shape variation decomposition and analysis of asymmetry. Entire landmark configurations were used, meaning we considered here the object symmetry of the head and mandibles as a whole. Individual shapes and their replicates were aligned by partial Generalized Procrustes Analysis, using functions from (Claude, 2008). Two different approaches were used in the decomposition of asymmetric variation. First, we implemented the approach from (Neubauer et al., 2020), with custom code, to obtain estimates of individual fluctuating asymmetry (iFA) and individual directional asymmetry (iDA) at the individual level. This relies on the use of non-centered PCA on the matrix of differences between the configuration of a given individual and its reflection across the sagittal plane. In the resulting PCA, the center of the space has a biological meaning, since it represents perfect symmetry (i.e. no difference between a configuration and its reflection). If the population average coordinate along one of the PC axes is significantly different from 0, it can be concluded that this axis represents DA variation. Individual positions (averaged across replicates) along this axis can therefore be used as a proxy for iDA in shape differences represented by this axis. When the population average along an axis is not different from 0 (and the distribution is not bimodal, which would suggest antisymmetry), the individual positions can serve as a proxy for iFA. In addition, individual total asymmetry (iTA) was also computed as the distance between a configuration and its reflection, averaged across replicates for the same individual. The second decomposition approach estimates DA and FA (as well as inter-individual variation) as population-level values, and relies on ANOVA (Palmer, 1994), as implemented in the geomorph R package (function bilat.symmetry) (Adams & Otárola-Castillo, 2013). The ANOVA has two explanatory factors, individual (representing inter-individual variance), side (or mirroring, representing DA), with their interaction representing FA. Finally, using replicates allows one to take into account the landmarking error, and to test for significance of DA and FA.

Modularity and integration analyses. Replicated landmark configurations for each individual were averaged, and the resulting shapes were used for all following analyses. In this study, we test variational modularity in a strict sense, i.e., whether the grasshopper head shows stronger covariation within than between given groups of traits / anatomical regions (Zelditch & Goswami, 2021). We did not use exploratory but confirmatory approaches to test for modularity. This entails defining *a priori* different modular partitions to be tested against the null hypothesis of no modularity, and tested against each other. Landmarks were sorted into six different partitions (Fig.

2): (i) a 2-modules “Head-Mandibles” partition, in which all landmarks placed on both left and right mandibles were gathered into one module, while all other landmarks, placed on the head capsule and sensory structures, formed the second module. (ii) a 3-modules “Head-Mandible-Sensory” partition, in which landmarks from both mandibles are one module, landmarks from sensory structures (eyes, antennae, ocelli), which are in the dorsal half of the head, are the second module, and landmarks from the ventral half of the head capsule and frons/clypeus as the third module. (iii) a 3-modules “Head-Mandibles asymmetric” partition in which landmarks from the left and right mandibles are two separate modules, while the rest (entire head) constitute the third module. (iv) a 4-modules “Head-Mandible asymmetric-Sensory” partition, in which left and right mandibles are separate modules, and head landmarks are split between the dorsal (i.e. sensory) and ventral regions. (v) a 2-modules “Ventral-Dorsal” partition, in which landmarks from both mandibles and the ventral part of the head form a single module, while the dorsal head (i.e. sensory) landmarks constitute the second module. (vi) a 2 modules “Half-Half” partition, in which the left half and right half of the head (with their respective mandibles) constitute separate modules, with midline landmarks excluded from the analysis. In addition, mandibles alone were also tested for left-right modularity. These different partitions were tested against the null hypothesis of no modularity, and ranked against each other using two of the most widely used current approaches: EMMLi (Evaluating modularity with maximum likelihood), implemented in the EMMLi v.0.0.3 package (Goswami & Finarelli, 2016), and CR (Covariance ratio), implemented in the geomorph v. 4.0.5 package (Adams, 2016; Adams & Collyer, 2016). Because EMMLi has been shown to have high false positive rates and to strongly favor models with more parameters (Adams & Collyer, 2019), we only show these results in details in the Supplementary Material. Integration between modules was also tested pairwise for each partition using two-block partial least squares (2B-PLS), as implemented in geomorph. Because discussions are ongoing about the impact of Procrustes superimposition on results of modularity and integration analyses (Cardini, 2019, 2023; Zelditch & Swiderski, 2023), we ran our modularity and integration tests and comparisons a second time, while applying a second "local" superimposition module by module. In other terms, the globally superimposed coordinates array was split into "module by module" arrays, which were individually superimposed again. These "module by module" arrays were then concatenated back together in an array of the same dimensions as the original one, and with landmarks in the same order, before running modularity tests and comparisons once more. Although this process entirely removes the anatomical spatial and size relationship between modules, it does not preclude analyses of remaining covariances (Cardini, 2019). We then compare results from both approaches (i.e. global superimposition and module by module superimposition).

Variability and correlations between bite force and asymmetry. To test whether the degree of asymmetry in the head and mandibles was functionally constrained, we assessed the correlation between individual *in vivo* maximum voluntary bite force (BF), and the various indices of individual asymmetry (iTA, iFA, iDA). One hypothesis was that the functional key-and-lock principle for good occlusion between mandibles would lead to an optimum asymmetry value maximizing bite forces, and therefore to a quadratic relationship between BF and iTA or iDA. On the other hand, FA is generally considered to worsen fitness, therefore possibly leading to a negative relationship between iFA and BF. Finally, to test whether these traits are under selection, we computed their respective coefficients of phenotypic variation (CV_p), which can be viewed as a measure of adaptive accuracy (Hansen et al., 2006; Pélabon & Hansen, 2008).

All statistical analyses were carried out in the R programming environment version 4.2.1.

Results

Head shape asymmetry. As expected, head shape at the population level was strongly directionally asymmetric (Table 1, Fig. 3). This directional asymmetry (DA) is however located mostly on the mandibles, with the incisivi (landmarks 18 to 23) being the most conspicuously asymmetric structures, as well as the insertion area of the mandible closer muscle (landmarks 28-29, 32-33; Fig. 3). DA can also be noticed in head structures which are located close to the mandibles, such as the clypeus-labrum region (landmarks 1-3 and 12), and the tentorial bridge (landmarks 14-15). The major directionally asymmetric patterns are the tilting of the clypeus-labrum region towards the right side, and the dorso-ventral and antero-posterior displacement of mandible incisivi. Fluctuating asymmetry (FA) is also significant, although its magnitude is much less than DA. FA is more spread out across the head than DA, however, the incisivi also show a higher FA (Supp. Fig. 1).

When using Neubauer et al.'s (2020) approach, the major asymmetric component, explaining over 90% of asymmetric variance, is directional (Fig. 4). The second axis, which represents about 2% of asymmetric variance is centered around 0 (One sample t-test, mean = 0.0021, t = 0.5208, df = 48, P = 0.6049), and normally distributed (Shapiro-Wilk normality test, W = 0.9885, P = 0.9105), suggesting it represents a FA component. Further axes, representing ≤1% of asymmetric variance were not explored. Unexpectedly, iFA and iDA (i.e. positions of individuals along these two asymmetric axes) appear correlated with each other (Fig.4, Pearson's correlation, r = 0.3569, t = 2.6191, df = 47, P = 0.0118). Similar results were obtained when restricting these analyses to landmarks from the mandibles only.

Modularity and integration. Both CR and EMMLi do not support the null hypothesis of no modularity in the grasshopper's head (Table 2, Supp. Table 1). EMMLi suggests the most likely modularity partition is the "Head-Mandibles asymmetric-Sensory" one (Fig. 2D), followed by the "Head-Mandibles asymmetric" one (Fig. 2C). On the other hand, the comparison between CR tests suggests the strongest modular signal is found in the simple 2-module "Head-Mandibles" partition (Fig. 2A). CR suggests that all modular partitions are significantly different from the null hypothesis of no modularity, but also that the strengths of modular signals between all those partitions are not significantly different from each other (Table 2). It should also be noted that the partition with the second largest modular effect is the most complex model, the 4 modules "Head-Mandibles asymmetric-Sensory" partition. When running the comparison of CR tests again after module-by-module superimposition, the Z_{CR} values are lower (i.e. modular signal gets stronger) overall. This is expected, as these "local" superimposition mathematically tend to add intra-module covariance, and reduce inter-module covariance. Again, all partitions are significantly different from the null hypothesis of no modularity (all $P < 0.001$), and again the differences between partitions in terms of modularity signal are not significant (all $P > 0.1$). The strongest modular signal (lowest Z_{CR}) is found, as with the global superimposition, in the 2-module "Head-Mandibles" partition, and the 4 modules "Head-Mandibles asymmetric-Sensory" partition also has strong modular signal (Fig. 5). It is however striking that the "Half-Half" partition, which has the weakest modular signal with the global superimposition, has on the other hand the second strongest signal in the module-by-module superimposition analysis.

Pairwise between-module integration analyses (Table 3, Fig. 6) show significant integration between modules in all partitions (all $P < 0.02$). Differences in integration signal between partitions are generally non-significant (Table 3). The exceptions are the "Half-Half" and "Mandibles only" partitions. The latter has significantly stronger integration than the "Head-Mandible", "Head-Mandibles-Sensory", "Head-Mandibles asymmetric", and "Head-Mandibles asymmetric-Sensory" partitions. The former is only significantly different from the "Head-Mandibles asymmetric" partition. Pairwise r-PLS correlation values from the different partitions (Fig. 6) are generally

stronger between spatially close structures. The "Ventral-Dorsal" partition clearly shows the weakest between-module correlation, while the "Half-Half" partition has the strongest one. It should however be noted that the latter excludes midline landmarks, meaning the r-PLS value cannot be directly compared to other partitions (conversely, Z_{PLS} values are standardized and can be compared). When using module by module superimposition, results are globally similar, with a fairly strong positive relationship between pairwise r-PLS values computed after global vs. module-by-module superimposition (Fig. 6, Supp. Fig. 2, $R^2 = 0.6783$, $P < 0.0001$). Integration signal is systematically weaker after module-by-module superimposition than after global superimposition. More importantly, these differences lead also to differences in significance (Supp. Fig. 2): while all tests were significant when using the global superimposition, with module-by-module superimposition, integration was not found to be significant in the "Head-Mandibles", the "Head-Mandibles-Sensory", and the "Ventral-Dorsal" partitions. All other partition had significant integration (all $P = 0.001$), but even in these cases, pairwise integration relationships between individual modules were not always the same as when using global superimposition.

Variability and correlation in bite force and asymmetry. *In vivo* bite force is correlated neither to iDA (Pearson's correlation, $r = -0.0102$, $t = -0.0691$, $df = 46$, $P = 0.9452$), nor to iFA ($r = 0.1138$, $t = 0.7771$, $df = 46$, $P = 0.4411$), nor to iTA ($r = 0.0244$, $t = 0.1657$, $df = 46$, $P = 0.8691$). Quadratic and linear model fits to the data were all non-significant (all $R^2 < 0.1$, all $P > 0.2$, Fig. 7). This result held whether we used iDA, iFA, iTA, or iDA restricted to only the mandibles. The coefficients of phenotypic variation (CV_p) were rather low for iTA ($CV_p = 0.1716$) and iDA ($CV_p = 0.2128$), slightly higher for bite force ($CV_p = 0.3147$), and very high for iFA ($CV_p = 1.2334$). For reference we also computed CV_p for head centroid size, which had a much lower value of $CV_p = 0.0506$.

Discussion

In this study, we showed large and significant directional asymmetry (DA) in the head of the grasshopper *Schistocerca gregaria* (Table 1, Fig. 4). Most of this directional asymmetry concentrates at the mandibles, as expected since they are conspicuously asymmetric structures, but also in surrounding head structures (Fig. 3). Fluctuating asymmetry (FA) was also significant, although accounting for much less variation than DA. Despite being more spread out than DA, the largest FA was also found in the mandibles. We also showed that the level of individual head asymmetry does not appear to influence individual biting performance (Fig. 7). Significant modularity was found, with the strongest modular signal in the 2 modules partition separating the head capsule (including sensory structures and the clypeus and labrum) from the mandibles (both sides combined) (Table 2, Fig. 5). While left and right mandible shapes are strongly correlated (Fig. 6), there appears nevertheless to be support for some degree of modularity between them (Table 2, Supp. Table 1). There is also support for significant modularity between the dorsal half of the head, holding the sensory structures, and the ventral half of the head, which appears more correlated to the mandibles (Fig. 6).

Linking conspicuous asymmetry with modularity.

Despite being recognized as a *tagma*, and therefore being an integrated anatomical unit (Minelli et al., 2013), our results show that the insect head is also to some extent variationally modular. This result fits with the fact that different parts of the head derive developmentally from various specialized segments (Posnien & Bucher, 2010), which are then used for different functions. Variational modularity patterns support the idea that the mandibles form a functional module for feeding, while the dorsal half of the head is a functional module for sensing. Within the feeding module, we also propose that, given our data, the conspicuously asymmetric mandible shapes are

best explained by developmental modularity between left and right sides. Indeed, both approaches used to test and compare modularity partitions of the head lend some support to the fact that the left and right mandibles each constitute a variational module (hypothesis (i) of the Introduction). While EMMLi strongly favors partitions in which left and right mandibles are separate modules (Fig. 2C-D), it should be noted that these are also partitions which have a large number of parameters to estimate (Supp. Table 1). As the EMMLi approach was shown to artificially favor partitions with more parameters (Adams & Collyer, 2019), this result may therefore be spurious. On the other hand, the CR modularity analyses also showed significant modularity in partitions which separate left and right mandibles (Table 2). Although these partitions are not the ones showing the strongest modularity scores, differences with other partitions are not significant. It therefore appears there is a degree, albeit limited, of variational autonomy between the left and right mandibles. Several factors may play a role in this autonomy: To achieve conspicuously different morphologies, left and right mandible developmental pathways must be neighbouring, but to some extent divergent (Meinhardt, 2001; Palmer, 2004). This divergence may in turn be a source of decorrelation between mandibles, allowing variable left-right differences, and causing slight variational modularity. Another, non-exclusive possibility is revealed by the relatively large magnitude of FA located at the mandible incisivi (Supp. Fig. 1). Because FA is of random direction, it may also reduce the correlation between left and right mandible shapes. However, the amount of variation explained by FA is very limited in comparison to DA, which would suggest that the influence of FA on modularity patterns is small.

Although mandibles have some degree of autonomy from each other, they remain strongly integrated (Fig. 6C-D, Table 3), and the strongest modular signal retrieved by the CR analysis is in the two modules partition which combines both mandibles into one module (Fig. 2A, Table 2), and the head structures in a second module. This suggests that the functional selection for matching left and right mandible shapes is limiting deviations from the left and right respective target phenotypes. In other terms, the developmental pathways for left and right mandibles must diverge at some point, but their combined target phenotype must be tightly integrated. This is corroborated by the relatively small CV_p of iTA and iDA, which fall in the range of values for characters under selection (Hansen et al., 2006; Pélabon & Hansen, 2008).

Variational modularity between the mandibles and the rest of the head might have been expected, considering that the mandibles constitute both a developmentally (Posnien & Bucher, 2010) and functionally distinct module. Our results constitute evidence that modularity between the head and the mandibles allows conspicuous asymmetry to appear in the mandibles while maintaining the head's global symmetry. This could potentially be a general rule in cases of conspicuous asymmetry arising in Bilaterians, where modularity may be an evolutionary way to relax locally the constraints of symmetry, akin to the more general idea that modularity may "favor evolvability by allowing one module to change without interfering with the rest of the organism" (Hansen, 2003). For the skull of toothed whales, it was suggested that it is asymmetry which drives modularity (Churchill et al., 2019). We instead propose that modularity is one prerequisite for conspicuous asymmetry to start evolving. This fits in our opinion better with the idea that modularity allows traits to evolve independently (Hansen, 2003; Zelditch & Goswami, 2021). It might also be the case that there are strong evolutionary positive feedbacks between modularity and asymmetry: for example, once conspicuously asymmetric structures appear, they may be used for divergent functions, which would entail disruptive selection, reinforcing integration *within* left and right structures and increasing modularity *between* them.

Additionally, the link between conspicuous asymmetry and modularity is probably dependent on the type of anatomical and functional relationships between left and right structures, and their

symmetrical surroundings. In the case of the grasshopper, mandibles are working together to achieve a single function, which certainly constrains the degree of modularity between left and right sides. In other cases, such as claws of lobsters or fiddler crabs, left and right functions are divergent, and one might therefore expect even stronger left-right autonomy, although there is data indicating significant linkage in dimorphic crab claws (Levinton, 2016). It should however be noted that such potential left-right autonomy does not necessarily entail differences in the level of within-side integration, and indeed no difference in integration was found in aeglid fighting and non-fighting claws (Nogueira et al., 2022). On the other hand, in cases where asymmetric structures are embedded within symmetric structures, such as the Cetacean skull, one may expect that the degree of modularity between them is reduced, compared to what we observe in our study. One may also expect that in more symmetrical species, e.g. insects with symmetrical mandibles, Mysticete whales which have symmetrical skulls, or crustaceans with symmetric claws, modularity should be smaller both between left and right sides, and between the studied structure and its anatomical surroundings. This idea is indirectly supported by results from Churchill et al. (2019), who found a larger number of modules in Odontocete whales skulls, compared to classical modularity patterns found in other mammals.

Asymmetry "spill-over" and modularity within the head capsule.

The modularity observed between the ventral and dorsal halves of the head may seem at first glance surprising, considering the head capsule is a rather continuous cuticular ensemble, in which junctions between segments are not visible anymore. The fact that DA is observed in the ventral half, and not in the dorsal half (hypothesis (iv) in the introduction, Fig. 3) may give us a hint. Indeed, asymmetrical mechanical loads from feeding may explain why structures in the ventral half of the head show large DA compared to the dorsal half. This functional linkage, related to the spatial proximity and anatomical articulation of mandibles of the ventral half of the head, could participate in the higher correlation between the ventral half of the head and the mandibles, compared with the correlation between the ventral and dorsal half of the head (Fig. 6D). It should also be mentioned that the very strong and asymmetric closer muscles of the mandibles in fact originate from the internal side of the dorsal part of the head (Weihmann & Wipfler, 2019). The limited DA observed in this dorsal region may therefore be explained by selection for maintenance of symmetry, related to the maintenance of optimal sensory performance, which could be achieved by reinforcements of the cuticle, as observed for example around the eyes with the circumoccular ridge as a reinforcing structure. Such selective constraint may not be as strong in the ventral half of the head, which does not have large sensory organs as on the dorsal head capsule.

Effect of module-by-module superimposition on modularity analyses.

There is ongoing discussion in the morphometrics community about the impact of Procrustes superimposition on modularity and integration results (Cardini, 2019, 2023; Zelditch & Swiderski, 2023). Previous studies tackling this problem relied heavily on simulations. Here, we analysed an empirical example by running CR analyses twice: first with one global superimposition, and second after applying a module-by-module superimposition. Reassuringly, the results are generally in agreement using both approaches, with all partitions showing significant modularity, and no significant differences between partitions. Furthermore, partitions with the highest modular signal are similar between both approaches, with one major difference in the "Half-Half" partition (Fig. 5) which has the lowest modular signal when using the global superimposition, but the second highest when using module by module superimposition. This phenomenon is most probably explained by

the loss of size relationships between halves in the module-by-module approach. Indeed, since one mandible is shorter than the other, but both halves of the head capsule are of similar size, when splitting the halves, the scaling step of Procrustes superimposition will therefore mostly be affected by the degree of asymmetry in the mandibles, causing decorrelation, and increasing modularity. This phenomenon had been anticipated (Cardini, 2019), and the loss of spatial and size relationships between modules explains that Z_{CR} values are almost always higher with the module-by-module superimposition. Regarding the integration results, although the degree of integration computed for the different partitions is correlated between the global and module by module approaches (Supp. Fig. 2), the agreement does not appear as good as for modularity. Indeed, while integration is always significant using the global superimposition, corroborating results from (Zelditch & Swiderski, 2023), only around half of the cases are significant when using module by module superimposition. Once again, this is certainly due to the fact that module by module superimposition necessarily removes spatial and size covariance between modules. However, it remains unknown how much of true biological covariance may also be lost in that process. We would argue that using module by module superimposition before integration analyses can therefore be taken as a conservative approach, lending strong confidence in the cases in which integration remains significant, although it may at the same time entail some false negative results.

Relationship between bite force performance and asymmetry.

Because left and right mandible shapes must fit each other to achieve their proper function, it could be expected that there exists an optimal asymmetric shape producing the best feeding performance. We therefore expected that there should be an optimal degree of directional asymmetry, deviations from which should reduce performance. We aimed at measuring this performance by recording maximum bite forces at the incisivi. Our results, however, clearly show no relationship between bite forces and directional, total or fluctuating asymmetry (Fig. 7). Because it may be argued that proper feeding performance may in fact leave room for a larger amount of variation in the fit of mandible shapes, we computed CV_P, which appears in accordance with the fact that iDA and iTA are indeed under selection, with values matching those for other selected characters reviewed by (Hansen et al., 2006). The absence of relationship revealed here may therefore have two explanations: (i) the degree of asymmetry may impact shearing forces and occlusion, but not static equilibrium bite forces at the tip of the incisivi, as we measure here, or (ii) because mandible shapes are selected to fit each other, variation in the degree of asymmetry is limited, while variation in bite force may be increased by other unrelated factors (for example environmental or experimental), which could explain why CV_P is higher for bite force than for iTA of iDA.

Conclusion and perspectives.

Modularity is often referred to as a mechanism which allows phenotypic diversification by allowing different anatomical parts to evolve in relative independence (Hansen, 2003; Zelditch & Goswami, 2021). Our results constitute some of the first evidence that modularity may indeed have a role in the evolution of disrupted symmetry, here in the head and mandibles of grasshoppers. This potential link between conspicuous asymmetry and modularity had, to our knowledge, only been suggested once before (Churchill et al., 2019), but never tested using separate left-right modules. Interestingly, one study also reported an asymmetric modular pattern in the context of hybridization (Parr et al., 2016), in non-conspicuously asymmetric animals (dogs and dingoes). This may hint at one possible way for conspicuous asymmetry to start appearing, with hybridization disrupting integration and modularity patterns within each species. Genetic assimilation has been suggested (Palmer, 1996, 2004) as another avenue for appearance of conspicuous asymmetry, which would not necessarily require modularity.

It is our opinion that exploring the link between conspicuous asymmetry and modularity is of interest in at least two broad evolutionary questions. First, conspicuous asymmetries and their evolution remain largely understudied compared to subtle asymmetries, particularly compared to FA. Understanding how ancestrally symmetrical structures can evolve to break the classical bilaterian symmetrical *bauplan* locally, while maintaining overall symmetry seems like a major, yet underexplored, aspect of phenotypic diversification (Palmer, 1996). Second, conspicuous asymmetries, which constitute a kind of "internal" diversification of homologous structures, would be a good model to test the idea that modularity is key in phenotypic diversification. This could be tested in at least three complementary ways: (i) By comparing modularity levels of the same structures between related species either showing conspicuous asymmetry or not, with the expectation that "asymmetric species" should show stronger left-right modularity as well as stronger modularity between symmetrical and asymmetrical structures, compared to "symmetric species". (ii) In species which have serially homologous structures, some of which are conspicuously asymmetric while others not (e.g. arthropod appendages), with the expectation that the asymmetrical structures would have stronger left-right modularity compared to their symmetrical serial homologs. (iii) Across clades and across structures, the strongest left-right modularity should be found in structures in which the left and right sides achieve different functions, intermediate modularity should be found in structures showing left-right differences allowing them to achieve a common function, and the lowest left-right modularity may be found in structures in which the left and right sides are physically tightly connected.

Figure legends

Figure 1. A.-B., G.-I. Location of the 35 landmarks used in the present study, illustrated on a colorized 3D reconstruction of a grasshopper head. A. Frontal view of the head as a whole. B. Ventral view of head capsule with mandibles, muscles and other internal organs removed. G.-I. Mandibular landmarks, illustrated for the left mandible (red), and its associated opener (pink), and closer (violet) muscles. Landmarks homologous to those shown here were also placed on the right mandible (not shown). G. Posterior view. H. Medial view. I. Anterior view. C.-F. Illustration of the mandibles in closed occluding position, displaying their key-and-lock morphology. C.-D. Posterior view, with and without transparency of the right mandible, respectively. E.-F. Anterior view, with and without transparency of the left mandible.

Figure 2. The various modularity partitions of landmarks tested and compared in this study. Dots represent landmarks, shown in frontal view, as reminded in A. by the underlaid picture of the grasshopper head. Landmark colours do not have any specific meaning, but distinguish between each individual module. White landmarks in F. are excluded from any module.

Figure 3. Lollipop graph illustrating directional asymmetry (DA) patterns in the grasshopper head. Red landmarks belong to the mandibles, while beige landmarks are placed on the head capsule and sensory structures. Black bars show the direction and magnitude of DA. Left panel shows the frontal view, while the right panel shows the ventral view, both combined illustrating DA patterns in all three dimensions. Numbers close to landmarks are here to help the reader matching corresponding landmarks in frontal and ventral view.

Figure 4. Non-centred PCA computed from difference matrices between landmark configurations and their respective mirror configurations. Each dot represents one individual, and the centre of the plot corresponds to perfect symmetry (i.e. no difference between a configuration and its mirror). The x axis represents purely directional variation, accounting for most of the asymmetric variation, while the y axis represents the first fluctuating asymmetry (FA) component. Other axes are not illustrated, but account for ≤1% of total asymmetric variation. Note the apparent correlation between the two axes.

Figure 5. Barplot comparing Z_{CR} values (i.e. modularity effect size) across the different modularity partitions tested in this study, and between module by module Procrustes superimposition (black bars) or global Procrustes superimposition (grey bars). Note that more negative values correspond to stronger modularity.

Figure 6. Module pairwise integration, as represented by r-PLS values. Colours do not have a specific meaning but distinguish between individual modules. The width of the grey lines connecting the centroid of each module (large dots) is proportional to the r-PLS values, which are also displayed as numbers. Large font numbers show r-PLS values computed after global superimposition, while underlying small font numbers show corresponding r-PLS values computed after module-by-module superimposition. Note the latter values are always smaller than the former, which is explained by the loss of spatial and size covariance after module-by-module superimposition. Note that r-PLS values are not standardized effect sizes, and should therefore not be compared between the different partitions.

Figure 7. Individual *in vivo* bite forces plotted against the various indices of individual asymmetry computed in our study. Dashed grey lines show non-significant fitted quadratic regressions.

519 Table 1. Results from the bilateral object symmetry shape ANOVA (Type I), using 1000 Randomized
520 Residual Permutations (RRPP) for significance testing.

	Df	SS	MS	Rsq	F	Z	Pr..F.
ind	48	0.14689	0.00306	0.24838	2.6422	-7.25098	1
side	1	0.3648	0.3648	0.61686	314.97456	3.36624	0.001
ind:side	48	0.05559	0.00116	0.09401	4.70964	14.47838	0.001
ind:side:replicate	98	0.0241	0.00025	0.04075			
Total	195	0.59138					

521

522

523 Table 2. Comparison of effect sizes (Z_{CR}) from CR modularity analyses.

A. Effect sizes (ZCR). Negative values represent stronger modular signal.

	No Modules	Head-Mandibles	Head-Mandibles-Sensory	Head-Mandibles asymmetric	Head-Mandibles asymmetric-Sensory	Ventral-Dorsal	Half-Half	Mandibles only
	0	-4.5	-3.34	-3.25	-4.13	-3.5	-2.21	-3.23

B. Pairwise differences in effect size.

No Modules	0	4.5	3.34	3.25	4.13	3.5	2.21	3.23
Head-Mandibles	4.5	0	0.16	0.01	0.13	0.19	1.59	0.43
Head-Mandibles-Sensory	3.34	0.16	0	0.12	0.26	0.31	1.24	0.24
Head-Mandibles asymmetric	3.25	0.01	0.12	0	0.12	0.18	1.31	0.35
Head-Mandibles asymmetric-Sensory	4.13	0.13	0.26	0.12	0	0.07	1.61	0.52
Ventral-Dorsal	3.5	0.19	0.31	0.18	0.07	0	1.51	0.54
Half-Half	2.21	1.59	1.24	1.31	1.61	1.51	0	1.03
Mandibles only	3.23	0.43	0.24	0.35	0.52	0.54	1.03	0

C. Pairwise P-values associated with pairwise differences in effect size.

No Modules	1	0	0	0	0	0	0.03	0
Head-Mandibles	0	1	0.88	0.99	0.9	0.85	0.11	0.67
Head-Mandibles-Sensory	0	0.88	1	0.9	0.79	0.76	0.22	0.81
Head-Mandibles asymmetric	0	0.99	0.9	1	0.91	0.86	0.19	0.72
Head-Mandibles asymmetric-Sensory	0	0.9	0.79	0.91	1	0.94	0.11	0.6
Ventral-Dorsal	0	0.85	0.76	0.86	0.94	1	0.13	0.59
Half-Half	0.03	0.11	0.22	0.19	0.11	0.13	1	0.31
Mandibles only	0	0.67	0.81	0.72	0.6	0.59	0.31	1

524

525

526 Table 3. Comparison of effect sizes (Z_{PLS}) from r-PLS integration analyses. Significant differences are
527 highlighted in bold.

A. Effect sizes (ZPLS) for each partition.

	Head-Mandibles	Head-Mandibles-Sensory	Head-Mandibles asymmetric	Head-Mandibles asymmetric-Sensory	Ventral-Dorsal	Half-Half	Mandibles only
	2.75624	4.18681	3.11687	4.01071	2.17762	5.15903	5.31365

B. Pairwise differences in ZPLS between partitions.

Head-Mandibles	0	0.18549	0.63877	0.00469	0.37715	1.57656	**2.10529**
Head-Mandibles-Sensory	0.18549	0	1.0292	0.23604	0.27588	1.63784	**2.21155**
Head-Mandibles asymmetric	0.63877	1.0292	0	0.80223	0.85547	**2.55307**	**3.04515**
Head-Mandibles asymmetric-Sensory	0.00469	0.23604	0.80223	0	0.41235	1.85817	**2.41466**
Ventral-Dorsal	0.37715	0.27588	0.85547	0.41235	0	0.79362	1.25629
Half-Half	1.57656	1.63784	**2.55307**	1.85817	0.79362	0	0.65754
Mandibles only	**2.10529**	**2.21155**	**3.04515**	**2.41466**	1.25629	0.65754	0

C. Pairwise P-values associated with pairwise differences in effect size.

Head-Mandibles	1	0.85284	0.52297	0.99626	0.70606	0.1149	**0.03527**
Head-Mandibles-Sensory	0.85284	1	0.30339	0.8134	0.78264	0.10146	**0.027**
Head-Mandibles asymmetric	0.52297	0.30339	1	0.42242	0.39229	**0.01068**	**0.00233**
Head-Mandibles asymmetric-Sensory	0.99626	0.8134	0.42242	1	0.68009	0.06314	**0.01575**
Ventral-Dorsal	0.70606	0.78264	0.39229	0.68009	1	0.42742	0.20901
Half-Half	0.1149	0.10146	**0.01068**	0.06314	0.42742	1	0.51083
Mandibles only	**0.03527**	**0.027**	**0.00233**	**0.01575**	0.20901	0.51083	1

528

529

Adams, D. C. (2016). Evaluating modularity in morphometric data: Challenges with the RV coefficient and a new test measure. *Methods in Ecology and Evolution*, *7*(5), 565–572. https://doi.org/10.1111/2041-210X.12511

Adams, D. C., & Collyer, M. L. (2016). On the comparison of the strength of morphological integration across morphometric datasets. *Evolution*, *70*(11), 2623–2631. https://doi.org/10.1111/evo.13045

Adams, D. C., & Collyer, M. L. (2019). Comparing the strength of modular signal, and evaluating alternative modular hypotheses, using covariance ratio effect sizes with morphometric data. *Evolution*, *73*(12), 2352–2367. https://doi.org/10.1111/evo.13867

Adams, D. C., & Otárola-Castillo, E. (2013). geomorph: An R package for the collection and analysis of geometric morphometric shape data. *Methods in Ecology and Evolution*, *4*(4), 393–399. https://doi.org/10.1111/2041-210X.12035

Babcock, L. E. (2005). Asymmetry in the fossil record. *European Review*, *13*(S2), 135–143. https://doi.org/10.1017/S1062798705000712

Ball, G. E. (1992). The Tribe Licinini (Coleoptera: Carabidae): A Review of the Genus-Groups and of the Species of Selected Genera. *Journal of the New York Entomological Society*, *100*(2), 325–380.

Benítez, H., Lemic, D., Villalobos-Leiva, A., Bažok, R., Órdenes-Claveria, R., Pajač Živković, I., & Mikac, K. (2020). Breaking Symmetry: Fluctuating Asymmetry and Geometric Morphometrics as Tools for Evaluating Developmental Instability under Diverse Agroecosystems. *Symmetry*, *12*(11), 1789. https://doi.org/10.3390/sym12111789

Brown, N. A., & Wolpert, L. (1990). The development of handedness in left/right asymmetry. *Development*, *109*(1), 1–9. https://doi.org/10.1242/dev.109.1.1

Cardini, A. (2019). Integration and Modularity in Procrustes Shape Data: Is There a Risk of Spurious Results? *Evolutionary Biology*, *46*(1), 90–105. https://doi.org/10.1007/s11692-018-9463-x

Cardini, A. (2023). *Shall we all adopt, with no worries, the 'within a configuration' approach in geometric morphometrics? A comment on claims that the effect of the superimposition and sliding on shape data is "not an obstacle to analyses of integration and modularity"*. EcoEvoRxiv.

Chapman, R. F. (1964). The structure and wear of the mandibles in some African grasshoppers. *Proceedings of the Zoological Society of London*, *142*(1), 107–122. https://doi.org/10.1111/j.1469-7998.1964.tb05157.x

Churchill, M., Miguel, J., Beatty, B. L., Goswami, A., & Geisler, J. H. (2019). Asymmetry drives modularity of the skull in the common dolphin (*Delphinus delphis*). *Biological Journal of the Linnean Society*, *126*(2), 225–239. https://doi.org/10.1093/biolinnean/bly190

Claude, J. (2008). *Morphometrics with R*. Springer.

Clissold, F. J. (2007). The Biomechanics of Chewing and Plant Fracture: Mechanisms and Implications. In *Advances in Insect Physiology* (Vol. 34, pp. 317–372). Elsevier. https://doi.org/10.1016/S0065-2806(07)34006-X

Clune, J., Mouret, J.-B., & Lipson, H. (2013). The evolutionary origins of modularity. *Proceedings of the Royal Society B: Biological Sciences*, *280*(1755), 20122863. https://doi.org/10.1098/rspb.2012.2863

del Castillo, D. L., Segura, V., Flores, D. A., & Cappozzo, H. L. (2016). Cranial development and directional asymmetry in Commerson's dolphin, *Cephalorhynchus commersonii commersonii*: 3D geometric morphometric approach. *Journal of Mammalogy*, *97*(5), 1345–1354. https://doi.org/10.1093/jmammal/gyw101

del Castillo, D. L., Viglino, M., Flores, D. A., & Cappozzo, H. L. (2017). Skull ontogeny and modularity in two species of *Lagenorhynchus*: Morphological and ecological implications. *Journal of Morphology*, *278*(2), 203–214. https://doi.org/10.1002/jmor.20629

Evans, K. M., Larouche, O., Watson, S.-J., Farina, S., Habegger, M. L., & Friedman, M. (2021). Integration drives rapid phenotypic evolution in flatfishes. *Proceedings of the National Academy of Sciences*, *118*(18), e2101330118. https://doi.org/10.1073/pnas.2101330118

Goswami, A., & Finarelli, J. A. (2016). EMMLi: A maximum likelihood approach to the analysis of modularity. *Evolution*, *70*(7), 1622–1637. https://doi.org/10.1111/evo.12956

Govind, C. K. (1989). Asymmetry in Lobster Claws. *American Naturalist*, *77*(5), 468–474.

Govind, C. K., & Blundon, J. A. (1985). Form and function of the asymmetric chelae in blue crabs with normal and reversed handedness. *The Biological Bulletin*, *168*(2), 321–331. https://doi.org/10.2307/1541244

Graham, J. H., Freeman, D. C., & Emlen, J. M. (1994). Antisymmetry, directional asymmetry, and dynamic morphogenesis. In T. A. Markow (Ed.), *Developmental Instability: Its Origins and Evolutionary Implications* (Springer Netherlands, Vol. 2, pp. 123–139). Kluwer Academic Publishers. https://doi.org/10.1007/978-94-011-0830-0_10

Hansen, T. F. (2003). *Is modularity necessary for evolvability? Remarks on the relationship between pleiotropy and evolvability*.

Hansen, T. F., Carter, A. J. R., & Pélabon, C. (2006). On Adaptive Accuracy and Precision in Natural Populations. *The American Naturalist*, *168*(2), 168–181. https://doi.org/10.1086/505768

Huggenberger, S., Leidenberger, S., & Oelschläger, H. H. A. (2017). Asymmetry of the nasofacial skull in toothed whales (Odontoceti). *Journal of Zoology*, *302*(1), 15–23. https://doi.org/10.1111/jzo.12425

Klingenberg, C. P. (2022). Shape asymmetry—What's new? *Emerging Topics in Life Sciences*, *6*(3), 285–294. https://doi.org/10.1042/ETLS20210273

Klingenberg, C. P., Badyaev, A. V., Sowry, S. M., & Beckwith, N. J. (2001). Inferring Developmental Modularity from Morphological Integration: Analysis of Individual Variation and Asymmetry in Bumblebee Wings. *The American Naturalist*, *157*(1), 11–23. https://doi.org/10.1086/317002

Klingenberg, C. P., McIntyre, G. S., & Zaklan, S. D. (1998). Left-right asymmetry of fly wings and the evolution of body axes. *Proceedings of the Royal Society B: Biological Sciences*, *265*, 1255–1259. https://doi.org/10.1098/rspb.1998.0427

Laeta, M., Oliveira, J. A., Siciliano, S., Lambert, O., Jensen, F. H., & Galatius, A. (2023). Cranial asymmetry in odontocetes: A facilitator of sonic exploration? *Zoology*, *160*, 126108. https://doi.org/10.1016/j.zool.2023.126108

608 Lanzetti, A., Coombs, E. J., Miguez, R. P., Fernandez, V., & Goswami, A. (2022). The ontogeny of
609 asymmetry in echolocating whales. *Proceedings of the Royal Society B: Biological Sciences*, *289*,
610 20221090. https://doi.org/10.1098/rspb.2022.1090

611 Lebrun, R. (2018). *MorphoDig, an open-source 3D freeware dedicated to biology* [Computer
612 software].

613 Levinton, J. S. (2016). Bilateral linkage of monomorphic and dimorphic limb sizes in fiddler crabs.
614 *Biological Journal of the Linnean Society*, *119*(2), 370–380. https://doi.org/10.1111/bij.12809

615 Macleod, C. D., Reidenberg, J. S., Weller, M., Santos, M. B., Herman, J., Goold, J., & Pierce, G. J.
616 (2007). Breaking symmetry: The marine environment, prey size, and the evolution of asymmetry in
617 cetacean skulls. *The Anatomical Record*, *290*(6), 539–545. https://doi.org/10.1002/ar.20539

618 Meinhardt, H. (2001). Organizer and axes formation as a self-organizing process. *International*
619 *Journal of Developmental Biology*, *45*, 177–188.

620 Minelli, A., Boxshall, G., & Fusco, G. (Eds.). (2013). *Arthropod Biology and Evolution: Molecules,*
621 *Development, Morphology*. Springer Berlin Heidelberg. https://doi.org/10.1007/978-3-642-36160-9

622 Møller, A. P. (1990). Fluctuating asymmetry in male sexual ornaments may reliably reveal male
623 quality. *Animal Behaviour*, *40*(6), 1185–1187. https://doi.org/10.1016/S0003-3472(05)80187-3

624 Neubauer, S., Gunz, P., Scott, N. A., Hublin, J.-J., & Mitteroecker, P. (2020). Evolution of brain
625 lateralization: A shared hominid pattern of endocranial asymmetry is much more variable in humans
626 than in great apes. *Science Advances*, *6*(7), eaax9935. https://doi.org/10.1126/sciadv.aax9935

627 Nogueira, C. S., da Silva, A. R., & Palaoro, A. V. (2022). Fighting does not influence the morphological
628 integration of crustacean claws (Decapoda: Aeglidae). *Biological Journal of the Linnean Society*,
629 *136*(1), 173–186. https://doi.org/10.1093/biolinnean/blac026

630 Palmer, A. R. (1994). Fluctuating asymmetry analyses: A primer. In T. A. Markow (Ed.),
631 *Developmental Instability: Its Origins and Evolutionary Implications* (Vol. 2, pp. 335–364). Springer
632 Netherlands. https://doi.org/10.1007/978-94-011-0830-0_26

633 Palmer, A. R. (1996). From symmetry to asymmetry: Phylogenetic patterns of asymmetry variation in
634 animals and their evolutionary significance. *Proceedings of the National Academy of Sciences*, *93*(25),
635 14279–14286. https://doi.org/10.1073/pnas.93.25.14279

636 Palmer, A. R. (2004). Symmetry Breaking and the Evolution of Development. *Science*, *306*(5697),
637 828–833. https://doi.org/10.1126/science.1103707

638 Palmer, A. R. (2016). What determines direction of asymmetry: Genes, environment or chance?
639 *Philosophical Transactions of the Royal Society B: Biological Sciences*, *371*(1710), 20150417.
640 https://doi.org/10.1098/rstb.2015.0417

641 Parr, W. C. H., Wilson, L. A. B., Wroe, S., Colman, N. J., Crowther, M. S., & Letnic, M. (2016). Cranial
642 Shape and the Modularity of Hybridization in Dingoes and Dogs; Hybridization Does Not Spell the
643 End for Native Morphology. *Evolutionary Biology*, *43*(2), 171–187. https://doi.org/10.1007/s11692-
644 016-9371-x

645 Pélabon, C., & Hansen, T. F. (2008). On the adaptive accuracy of directional asymmetry in insect wing
646 size. *Evolution*, *62*(11), 2855–2867. https://doi.org/10.1111/j.1558-5646.2008.00495.x

Pither, J., & Taylor, P. D. (2000). Directional and fluctuating asymmetry in the black-winged damselfly *Calopteryx maculata* (Beauvois) (Odonata: Calopterygidae). *Canadian Journal of Zoology*, *78*(10), 1740–1748. https://doi.org/10.1139/z00-130

Posnien, N., & Bucher, G. (2010). Formation of the insect head involves lateral contribution of the intercalary segment, which depends on Tc-labial function. *Developmental Biology*, *338*(1), 107–116. https://doi.org/10.1016/j.ydbio.2009.11.010

Pratt, A. E., & Mclain, D. K. (2002). Antisymmetry in male fiddler crabs and the decision to feed or breed. *Functional Ecology*, *16*(1), 89–98. https://doi.org/10.1046/j.0269-8463.2001.00605.x

Püffel, F., Johnston, R., & Labonte, D. (2023). A biomechanical model for the relation between bite force and mandibular opening angle in arthropods. *Royal Society Open Science*, *10*, 221066.

Rühr, P., & Blanke, A. (2022). ForceX and ForceR: A mobile setup and R package to measure and analyse a wide range of animal closing forces. *Methods in Ecology and Evolution*, *13*(9), 1938–1948. https://doi.org/10.1111/2041-210X.13909

Savriama, Y., Vitulo, M., Gerber, S., Debat, V., & Fusco, G. (2016). Modularity and developmental stability in segmented animals: Variation in translational asymmetry in geophilomorph centipedes. *Development Genes and Evolution*, *226*(3), 187–196. https://doi.org/10.1007/s00427-016-0538-3

Tiwari, S., Nambiar, S., & Unnikrishnan, B. (2017). Chewing side preference—Impact on facial symmetry, dentition and temporomandibular joint and its correlation with handedness. *Journal of Orofacial Sciences*, *9*(1), 22. https://doi.org/10.4103/jofs.jofs_74_16

Van Valen, L. (1962). A Study of Fluctuating Asymmetry. *Evolution*, *16*(2), 125–142.

Wagner, G. P., Pavlicev, M., & Cheverud, J. M. (2007). The road to modularity. *Nature Reviews Genetics*, *8*(12), 921–931. https://doi.org/10.1038/nrg2267

Zelditch, M. L., & Goswami, A. (2021). What does modularity mean? *Evolution & Development*, *23*(5), 377–403. https://doi.org/10.1111/ede.12390

Zelditch, M. L., & Swiderski, D. L. (2023). Effects of Procrustes Superimposition and Semilandmark Sliding on Modularity and Integration: An Investigation Using Simulations of Biological Data. *Evolutionary Biology*, *50*(2), 147–169. https://doi.org/10.1007/s11692-023-09600-9

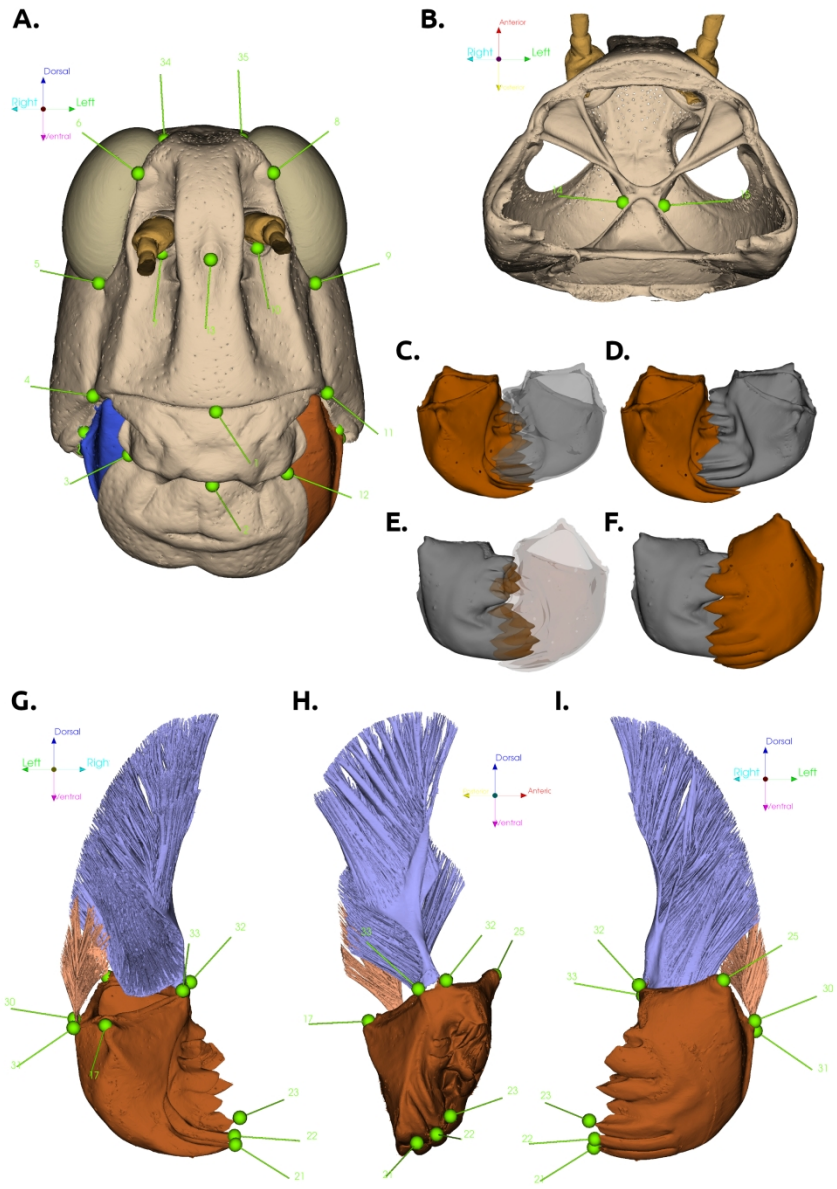

Figure 1. A.-B., G.-I. Location of the 35 landmarks used in the present study, illustrated on a colorized 3D reconstruction of a grasshopper head. A. Frontal view of the head as a whole. B. Ventral view of head capsule with mandibles, muscles and other internal organs removed. G.-I. Mandibular landmarks, illustrated for the left mandible (red), and its associated opener (pink), and closer (violet) muscles. Landmarks homologous to those shown here were also placed on the right mandible (not shown). G. Posterior view. H. Medial view. I. Anterior view. C.-F. Illustration of the mandibles in closed occluding position, displaying their key-and-lock morphology. C.-D. Posterior view, with and without transparency of the right mandible, respectively. E.-F. Anterior view, with and without transparency of the left mandible.

533x755mm (118 x 118 DPI)

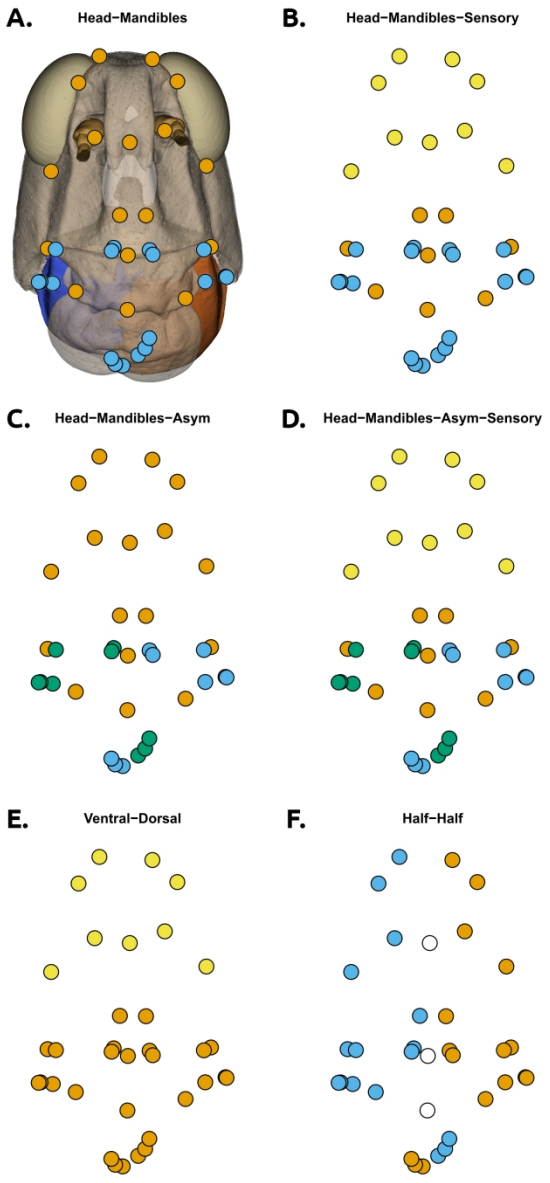

Figure 2. The various modularity partitions of landmarks tested and compared in this study. Dots represent landmarks, shown in frontal view, as reminded in A. by the underlaid picture of the grasshopper head. Landmark colours do not have any specific meaning, but distinguish between each individual module. White landmarks in F. are excluded from any module.

387x774mm (118 x 118 DPI)

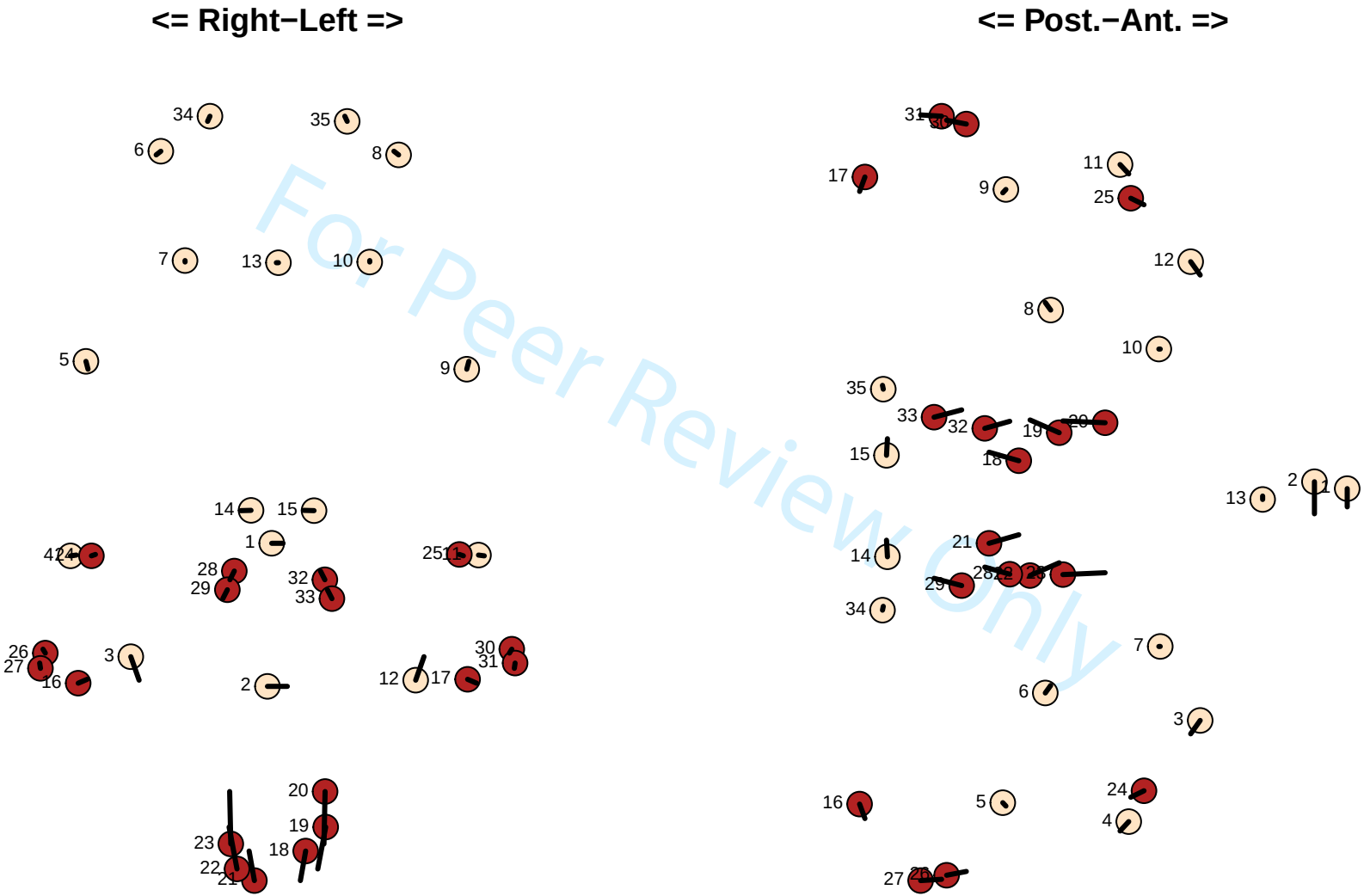

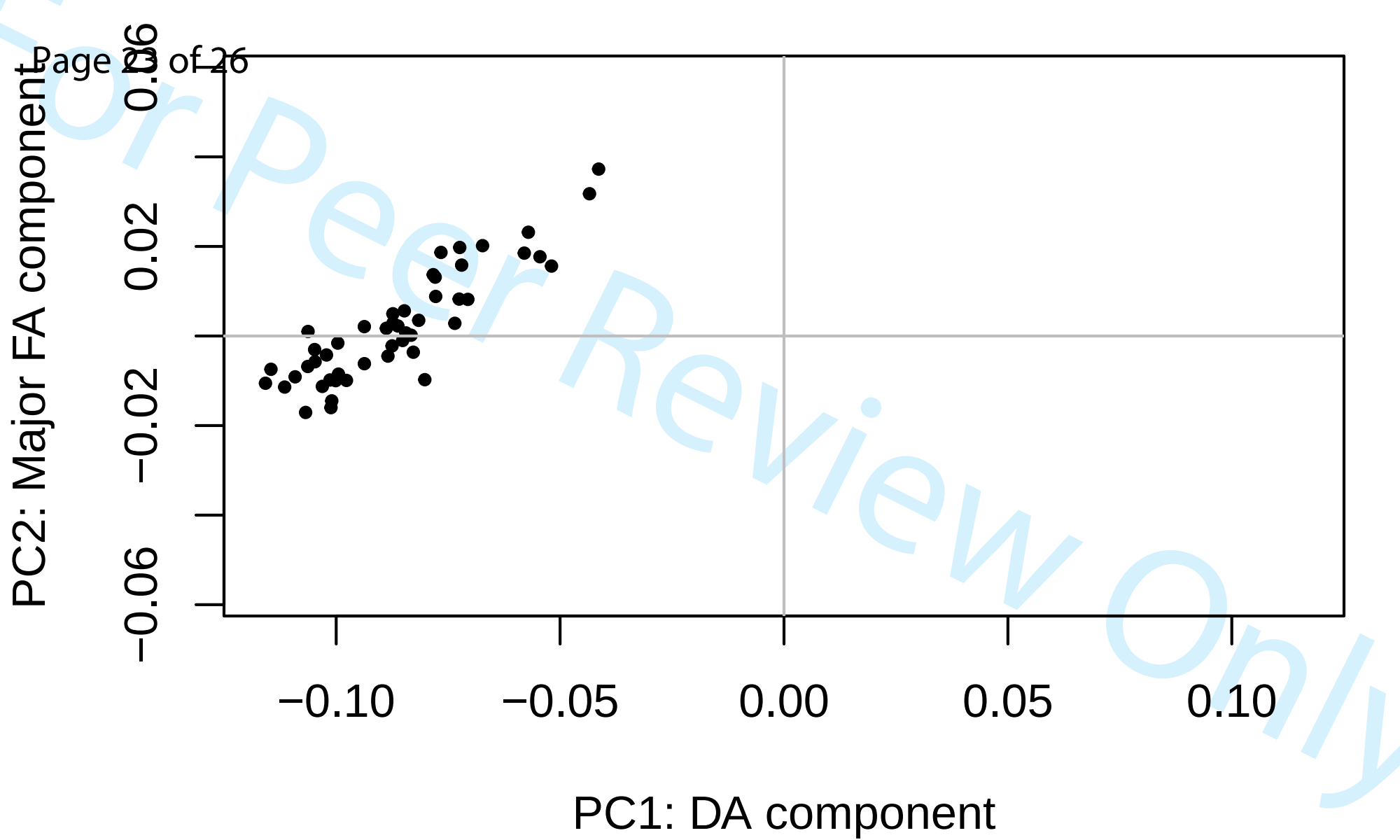

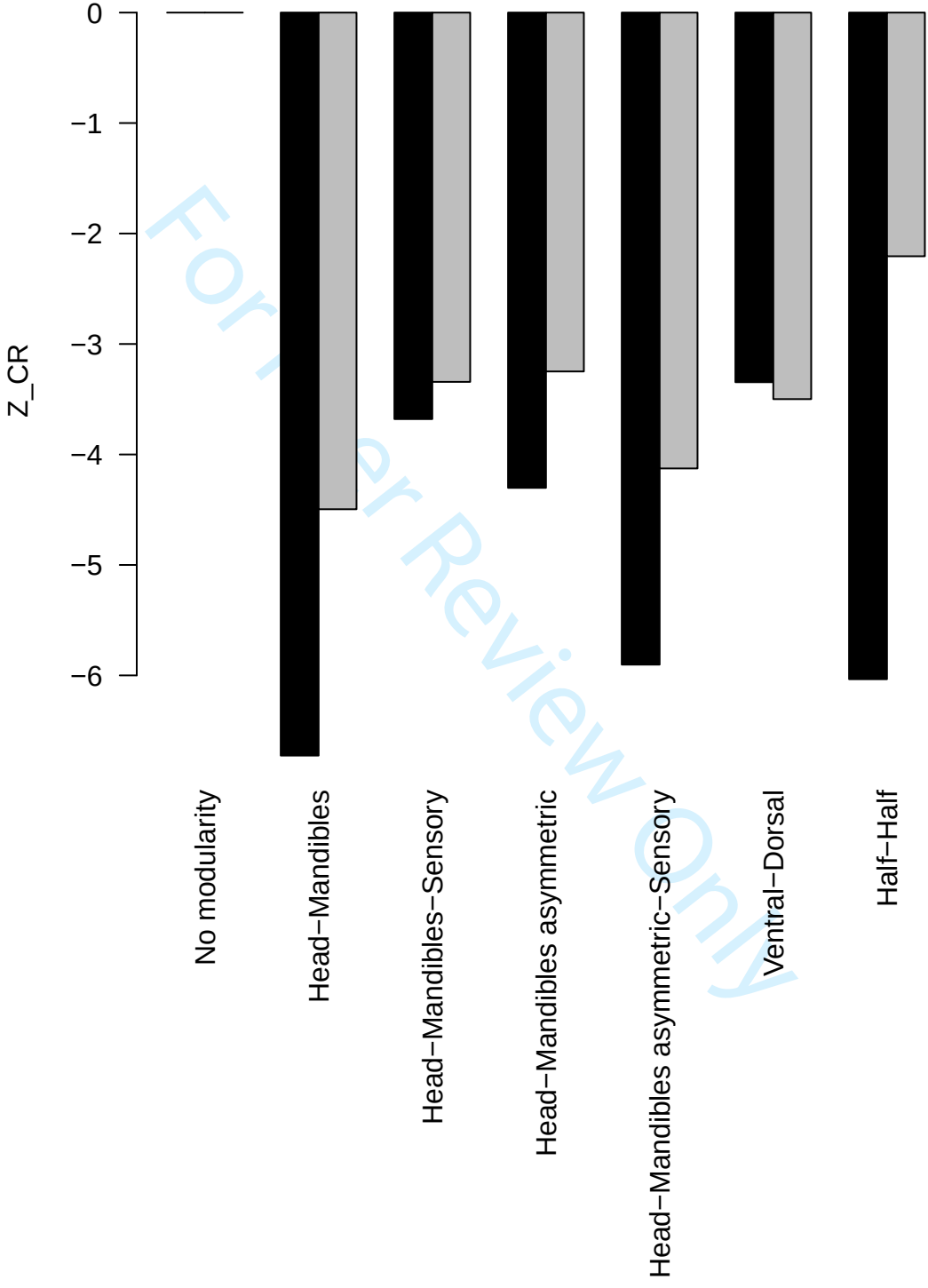

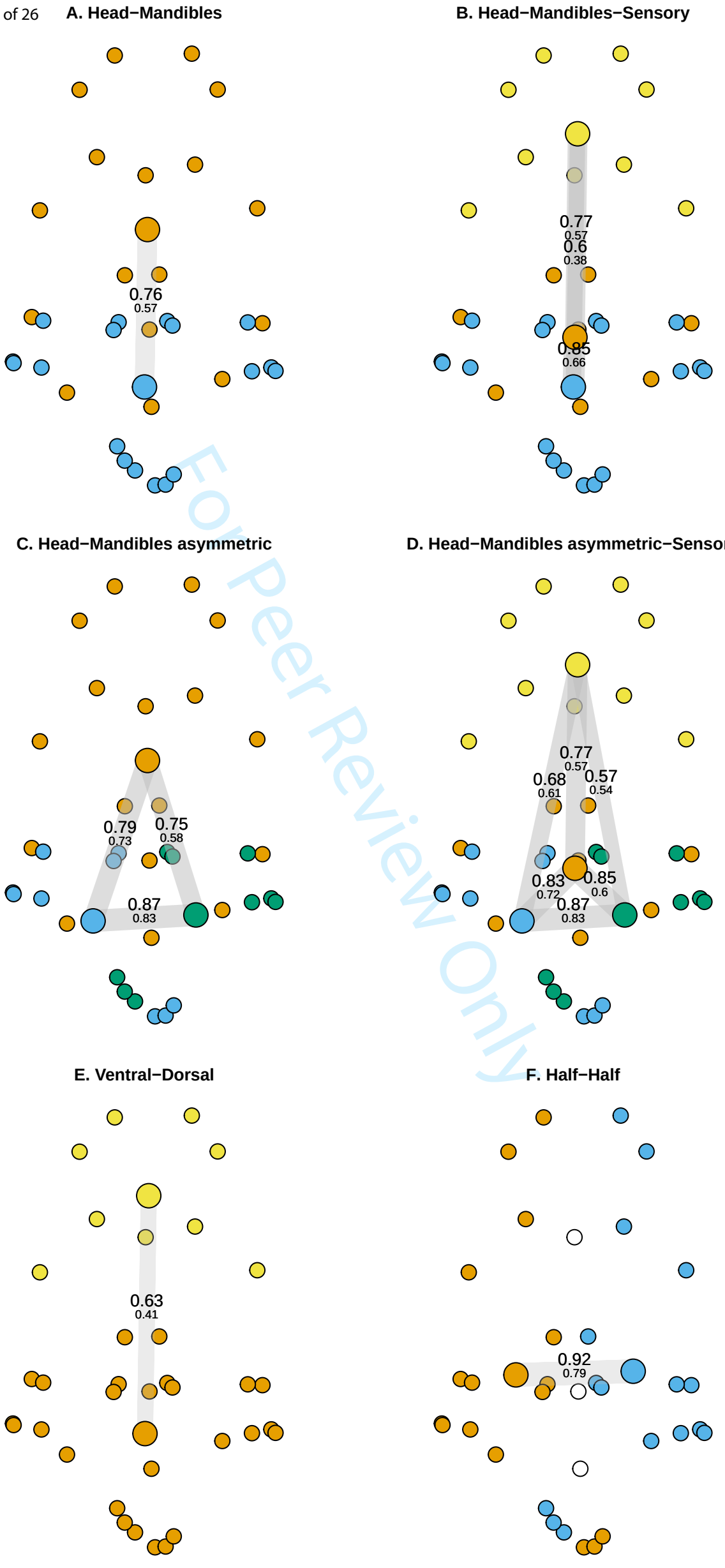

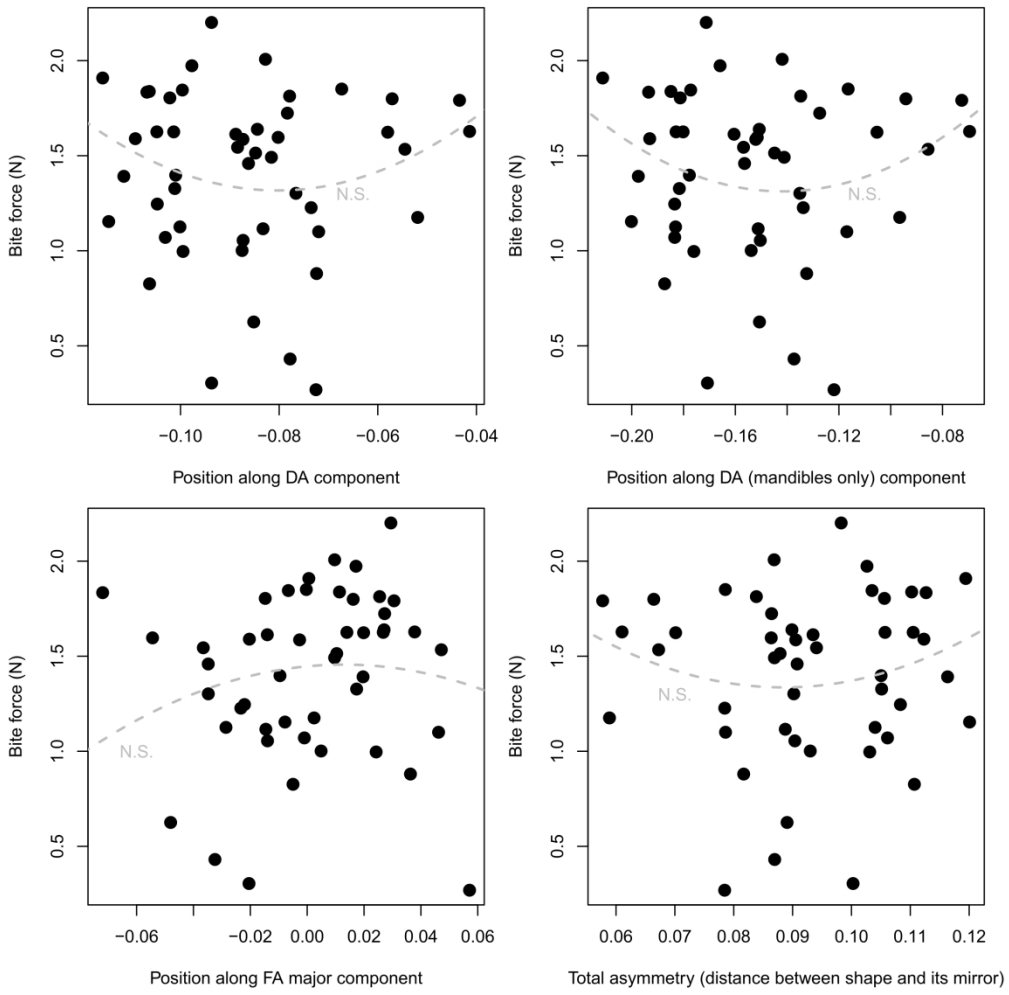

Figure 7. Individual in vivo bite forces plotted against the various indices of individual asymmetry computed in our study. Dashed grey lines show non-significant fitted quadratic regressions.

516x516mm (118 x 118 DPI)